JMEPEG (2018) 27:2772–2781
https://doi.org/10.1007/s11665-018-3388-5

©ASM International
1059-9495/$19.00

Effects of Controlled Cooling-Induced Ferrite–Pearlite Microstructure on the Cold Forgeability of XC45 Steel

Chengliang Hu, Lunqiang Chen, Zhen Zhao, Aijun Gong, and Weibing Shi

(Submitted July 22, 2017; in revised form January 6, 2018; published online May 3, 2018)

The combination of hot/warm and cold forging with an intermediate controlled cooling process is a promising approach to saving costs in the manufacture of automobile parts. In this work, the effects of the ferrite–pearlite microstructure, which formed after controlled cooling, on the cold forgeability of a medium-carbon steel were investigated. Different specimens for both normal and notched tensile tests were directly heated to high temperature and then cooled down at different cooling rates, producing different ferrite volume fractions, ranging from 6.69 to 40.53%, in the ferrite–pearlite microstructure. The yield strength, ultimate tensile strength, elongation rate, percentage reduction of area, and fracture strain were measured by tensile testing. The yield strength, indicating deformation resistance, and fracture strain, indicating formability, were used to evaluate the cold forgeability. As the ferrite volume fraction increased, the cold forgeability of the dual-phase ferritic–pearlitic steel improved. A quantitatively relationship between the ferrite volume fraction and the evaluation indexes of cold forgeability for XC45 steel was obtained from the test data. To validate the mathematical relationship, different tensile specimens machined from real hot-forged workpieces were tested. There was good agreement between the predicted and measured values. Our predictions from the relationship for cold forgeability had an absolute error less than 5%, which is acceptable for industrial applications and will help to guide the design of combined forging processes.

Keywords controlled cooling, ferrite, forgeability, fracture strain, microstructure, volume fraction, yield strength

1. Introduction

For fabrication of complex automobile parts, the combined hot/warm and cold forging process has become widely adopted (Ref 1, 2). Hot/warm forging can be used to obtain complex shapes though large deformations, while cold forging is used to achieve high-dimensional accuracy requirements. Different cold forging processes, including cold ironing (Ref 3) and compressing finishing (Ref 4), have been investigated experimentally and by finite element simulations. These results have shown that the specific dimensions and a greatly improved surface finish can be achieved through the use of cold forging as a post-process after hot/warm forging. In this work, a flange shaft was formed by three-stage hot forging together with a cold ironing process. With forward extrusion, upsetting, and backward extrusion, the complex shape was hot-forged, and the well-defined length of the flange shaft was achieved by cold ironing, as shown in Fig. 1.

The use of residual energy from hot/warm forging is a promising way to shorten the production line, which would result in cost savings for automobile part manufacture. Following the controlled rolling process, a controlled cooling process is used to make raw materials like carbon steel (Ref 5), low-carbon alloyed steel (Ref 6), and medium-carbon microalloyed (Ref 7) steel in bar or pipe shapes. Controlled cooling has already been shown to be effective in taking advantage of residual heat from hot working.

For medium-carbon structural steel, which is widely used in automotive parts, different microstructures including ferrite–pearlite, ferrite–martensite, and ferrite–bainite can be produced by different heat treatments. The mechanical properties of the corresponding dual-phase steels have been investigated. An increase in the amount of pearlite in the microstructure has a marked effect on the ferrite–pearlite steel deformation and failure properties (Ref 8). The yield strength, ultimate tensile strength (UTS), and work hardening decrease linearly with increasing ferrite volume fraction in ferrite–bainite steel of AISI 4340 (Ref 9). Ferrite–martensite steel has better ductility and Charpy impact energy but a lower yield and tensile strength than those of ferrite–bainite steel (Ref 10).

To replace these costly heat treatments (quenching and tempering) after forging with a controlled cooling from forging temperature in air, medium-carbon microalloyed steels have been developed. By increasing the cooling rate, the as-formed ferritic–pearlitic microstructure changes to acicular ferrite, bainite or martensite of a commercial microalloyed forging steel 30MSV6 (Ref 11). As the forged strain increases, the grade of austenite grain size increases at cooling rates of 1.5 and 2.5 °C/s (Ref 12). Results from shear punch tests show that both the yield and ultimate strength increase; however, the ductility decreases considerably as the cooling rate increases (Ref 11). Compared with air cooling, spray cooling processes can improve the proof stress and ultimate strength of a microalloyed steel 38MnVS6 (Ref 13). However, the medium-carbon microalloyed steel is not well promoted because its price is higher than that of medium-carbon structural steel.

In this work, the combined hot/warm and cold forging processes were studied. A controlled cooling process after the hot/warm forging was investigated, and the cold forgeability of

Chengliang Hu, Lunqiang Chen, and **Zhen Zhao**, Institute of Forming Technology and Equipment, School of Materials Science and Engineering, Shanghai Jiao Tong University, Shanghai 200030, China; **Aijun Gong** and **Weibing Shi**, Jiangsu Sunway Precision Forging Co, Ltd., Dafeng 224100, China. Contact e-mails: clhu@sjtu.edu.cn and zzhao@sjtu.edu.cn.

Fig. 1 Combined forging process of a flange shaft. (a) Billet, (b) three-stage hot forging, (c) cold ironing

a workpiece for a medium-carbon steel from controlled cooling was evaluated. From these results, we determined guidelines for the deformation degree following cold forging. These guidelines will allow effective combined hot–cold forging processes to be designed and give a good description of the distribution of deformation extent between the different forging stages.

In the present study, the effect of the ferrite–pearlite microstructure, after controlled cooling of a workpiece, on its cold forgeability was investigated. As reported in a previous study, the ferrite volume fraction in the microstructure of medium-carbon steel after controlled cooling is markedly affected by warm deformation parameters and cooling rates (Ref 14). Hence, in our current study the ferrite volume fraction was selected as a quantitative indicator to describe the corresponding microstructure. We investigated mechanical properties including yield strength, UTS, elongation rate, percentage reduction of area (PRA), and fracture strain by normal and notched tensile testing. The yield strength and fracture strain were used to evaluate the cold forgeability. On the basis of our experimental data, the mathematical relationship between the ferrite volume fraction and evaluation indexes of cold forgeability for XC45 steel was created. Finally, different tensile specimens from actual hot-forged workpieces of a flange shaft were made to test and validate the relationship.

2. Experimental

2.1 Material and Continuous Cooling Transformation Curves

We investigated an XC45 steel, which is almost the same as AISI 1045 and ISO IC45e used for flange shafts. This kind of medium-carbon steel is extensively applied in automobile parts. The typical chemical composition (mass percentage) was 0.46% C, 0.33% Si, 0.77% Mn, 0.013% P, 0.015% S, 0.04% Ni, and the reminder was Fe. The A1 and A3 temperatures of this steel can be determined as 724 and 780 °C with an assumed average grain size of 30 μm by using the TTT–CCT diagram generator in FORGE software (Ref 15). To understand the basic phase transformation behavior of XC45 steel, a brief static continuous cooling transformation diagram was constructed, as shown in Fig. 2(a). When the cooling rate is less than 5 °C/s, the microstructure is composed of ferrite and pearlite. However, a cooling rate of 20 °C/s results in the formation of some bainite, as shown in Fig. 2(b). A microstructure containing bainite is unfavorable for cold forming.

2.2 Experimental Approach and Procedures

2.2.1 Experimental Approach. To study the effects of the cooling rate after hot deformation on the microstructure and mechanical properties of the forging steel, the optical microscopy and shear punch testing (Ref 16) were performed. After deformation, the specimens in the slice shape were sectioned perpendicular to the deformation direction to introduce a strain effect into the final property (Ref 11). However, the strain distribution of the specimens after hot compression was consistently non-uniform (Ref 17). A high-level pre-strain, which can simulate the practical large deformation occurring during hot forging, is difficult to achieve in the following mechanical tests.

As shown in Fig. 3 (Ref 14), the ferrite volume fraction markedly increased with increasing strain at the same deformation temperature and also differed at different cooling rates of the medium-carbon alloyed steel. Thus, the variation of the ferrite volume fraction in the microstructure reflected changes of the strain history of the warm/hot deformation.

Tensile testing is a typical method for evaluating the plastic index of a material, but these test results have low accuracy owing to neck formation (Ref 18, 19). The notched tensile test, which involves a tri-axial pressure state and almost no necking phenomenon at the notched zone, proved to be a useful tool for determining the cold forgeability (Ref 19). In these tests, the value of the reduction in the section area was taken into consideration (Ref 20). Therefore, an experimental approach was proposed as follows: Specimens for both normal and notched tensile tests were directly heated to a high temperature and then cooled down at different cooling rates. Then, the different tensile tests were performed in sequence. On the basis of this experimental design, microstructures with different ferrite volume fractions and their corresponding forgeability could be investigated.

2.2.2 Experimental Procedure. A servo-controlled Gleeble 1500 system was used to conduct the heating and cooling processes. To simulate the real pre-heating process in forging, all the specimens were first heated to 1000 °C at 10 °C/s and held at that temperature for 3 min to enable complete austenitization. The specimens were then cooled to 950 °C at 5 °C/s and held at that temperature for 30 s. To reduce the risk of cracking caused by uneven heating and cooling and the effects of thermal expansion and shrinkage, the temperature distribution in the testing zone was controlled to be as uniform as possible. According to the CCT curves presented in Fig. 2, the maximum cooling rate was limited to 5 °C/s to guarantee a mixture of ferrite and pearlite in the microstructure. In the experiments, the heated specimens were cooled at seven different cooling rates of 5, 2, 1.5, 1, 0.5, 0.2, and 0.1 °C/s. For each cooling rate, three normal and three notched specimens were prepared, as shown in Fig. 4. Normal tensile testing is the most commonly used for obtaining the mechanical characteristics of isotropic materials, and the capability of plastic deformation for a material can be evaluated. Fracture strain from the notched tensile test has been previously used as an indicator for cold forgeability in Ref 19. Then, the corresponding tensile tests were performed at a speed of 2 mm/min using a Zwick testing machine.

From the normal tensile testing results, the yield strength, UTS, and elongation rate were directly measured. The PRA was calculated by measuring the diameter of the necking zone.

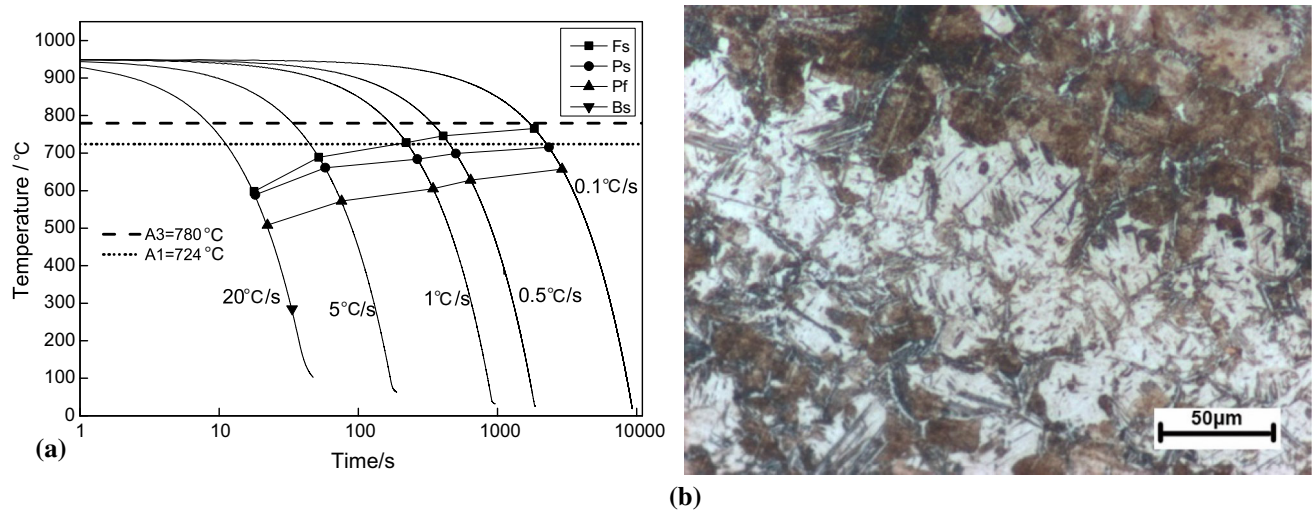

Fig. 2 CCT curves (a) and microstructure of XC45 steel (b) at cooling rate of 20 °C/s

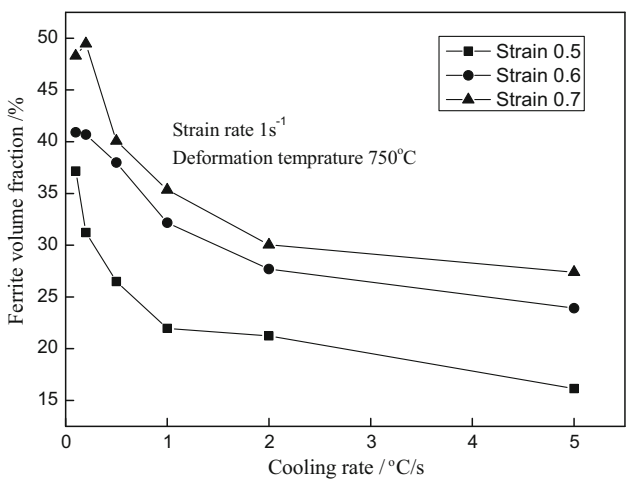

Fig. 3 Ferrite volume fraction from samples with different strain histories at different cooling rates (Ref 14)

From the notched tensile tests, the fracture strain was calculated as follows (Ref 19):

$$\varepsilon_f = 2\ln(d_0/d_f) \quad \text{(Eq 1)}$$

where d_0 and d_f are the initial diameter and the diameter at the fracture point of the notched specimens, respectively.

After the tensile tests, metallographic samples were prepared from broken specimens and etched with a 4% nital solution. The different microstructures were imaged with an optical microscope, and the corresponding ferrite volume fraction was determined by image processing through iterative binarization, median filtering, and volume calculation steps (Ref 14).

3. Results and Discussion

3.1 Microstructure Analysis

The microstructures of the different specimens at different cooling rates were a mechanical mixture of ferrite and pearlite.

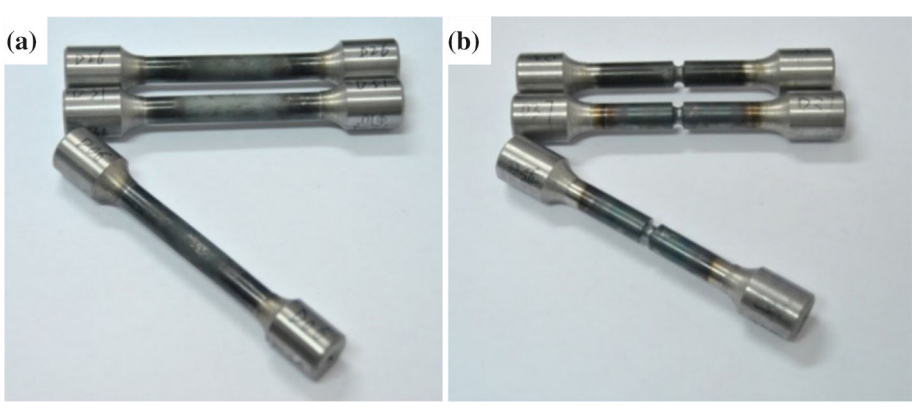

Fig. 4 Specimens for tensile tests: (a) normal; (b) notched

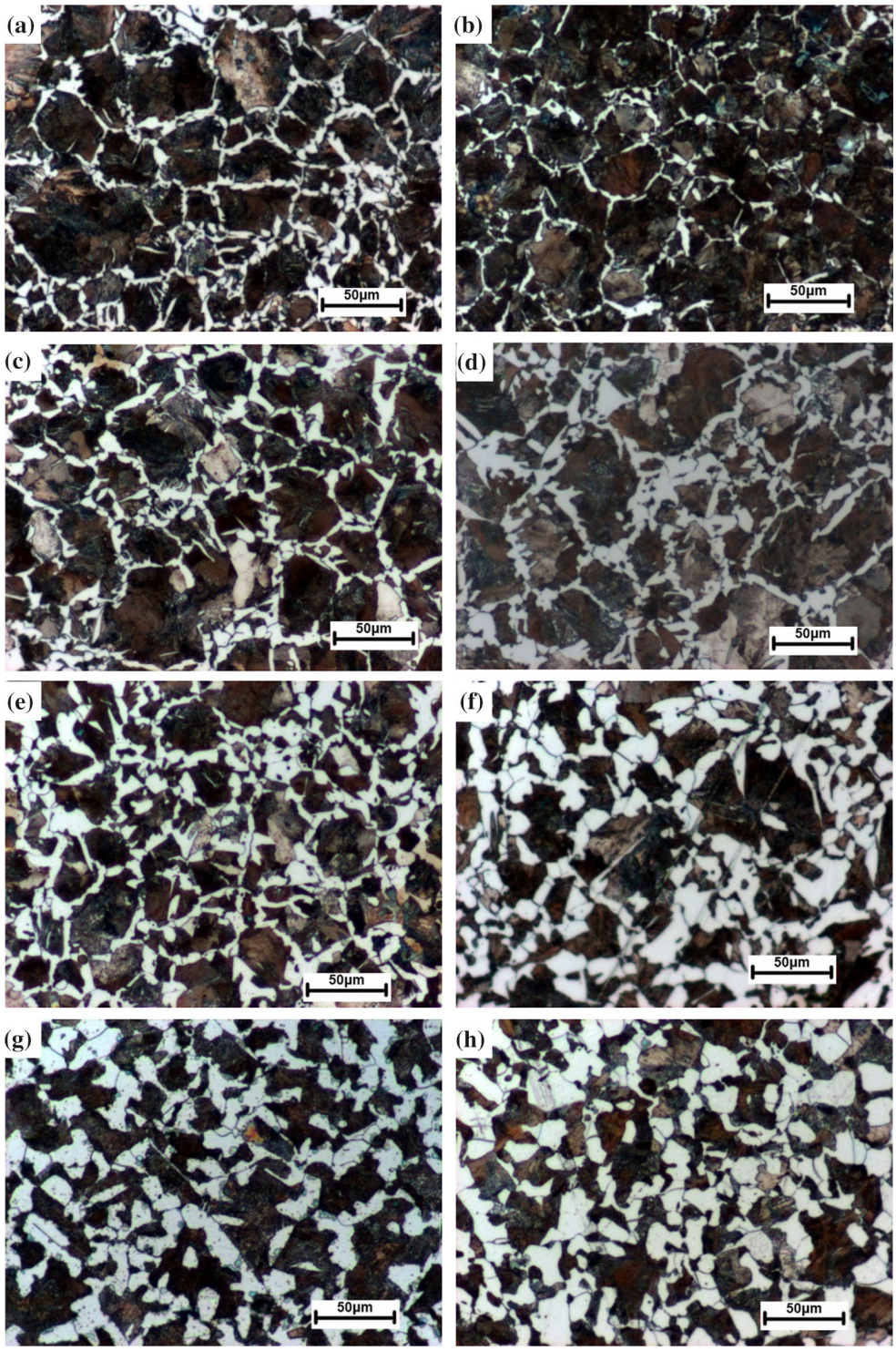

Fig. 5 Microstructures of tensile specimens at cooling rates of (a) 5.0 °C/s—normal, (b) 5.0 °C/s—notched, (c) 2.0 °C/s—normal, (d) 1.5 °C/s—notched, (e) 1.0 °C/s—normal, (f) 0.5 °C/s—notched, (g) 0.2 °C/s—normal, (h) 0.1 °C/s—notched

Even with a large cooling rate of 5 °C/s, dual-phase microstructures appeared as expected according to the above CCT curves, as shown in Fig. 5(a) and (b). During the phase transformation, proeutectoid ferrite initially nucleated along the boundaries of austenite grains and the retained austenite then transformed to pearlite as a result of eutectoid decomposition when the temperature decreased to a critical value. Finally, a mechanical mixture of ferrite and pearlite was formed (Ref 21). The grain size of ferrite was highly dependent on the primary austenite grain size and the cooling rate. The morphology of ferrite, as a high-temperature prevenient phase, determined the following distribution of pearlite (Ref 5). When the cooling rate was greater than 1.5 °C/s, the proeutectoid ferrite appeared to be a thin continuous network at the boundaries of former austenite grains, as shown in Fig. 5(a), (b), and (c). A high cooling rate led to a large degree of undercooling, and the

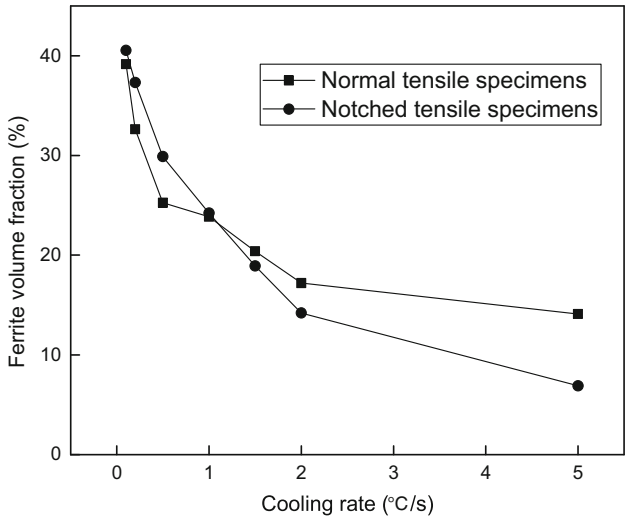

Fig. 6 Ferrite volume fractions of normal and notched tensile specimens formed at different cooling rates

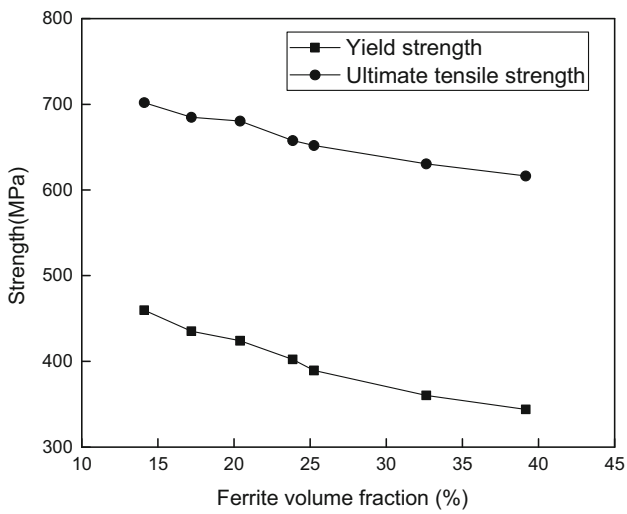

Fig. 7 Variation of yield strength and ultimate tensile strength with ferrite volume fraction

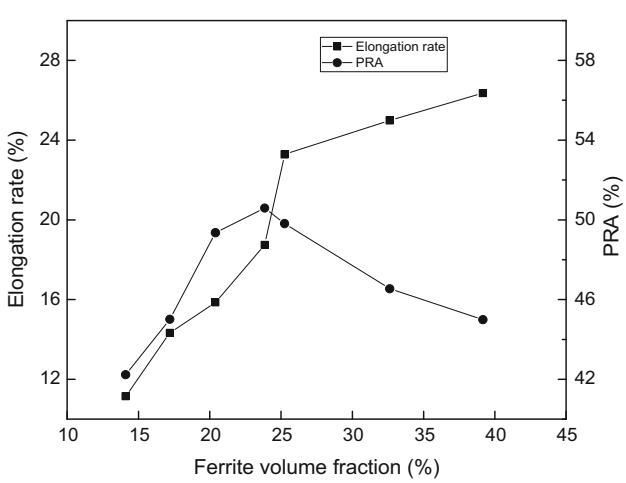

Fig. 8 Variation of elongation and percentage reduction of area with ferrite volume fraction

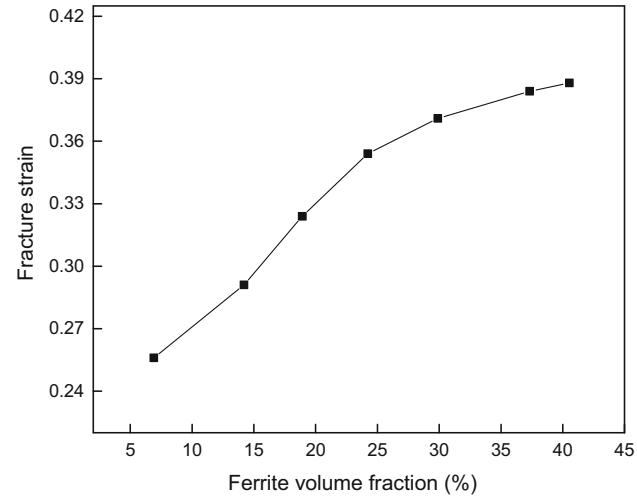

Fig. 9 Variation of fracture strain with ferrite volume fraction

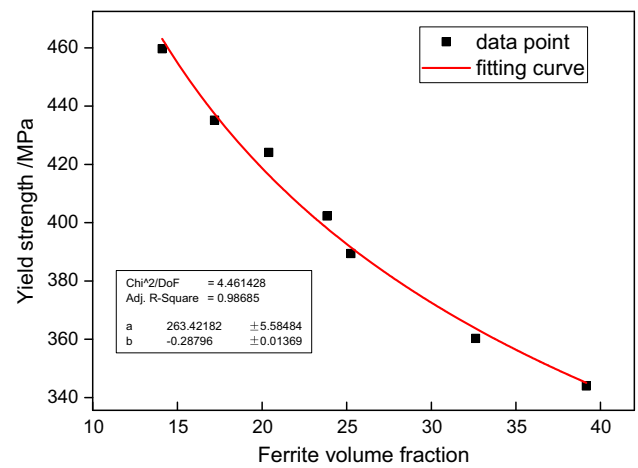

Fig. 10 Fitting process between yield strength and ferrite volume fraction

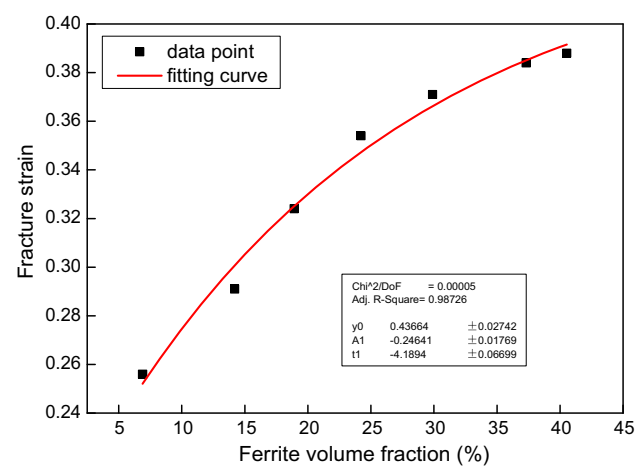

Fig. 11 Fitting process between fracture strain and ferrite volume fraction

transformation rate from austenite to ferrite was reduced to form fine ferrite by intergranular nucleation (Ref 22). Consequently, the undercooling matrix promoted the nucleation of pearlite. When the cooling rate was lower than 1.5 °C/s, many equiaxed grain geometries appeared in the microstructure, referred to as polygonal ferrite, as shown in Fig. 5(e), (f), (g), and (h). The ferritic microstructure, which formed at a high temperature and slow cooling rate, nucleated as grain-boundary allotriomorphs and grew into equiaxed grains (Ref 21). As a result, a more uniform distribution of the polygonal ferrite was obtained at a lower cooling rate, as shown in Fig. 5(g) and (h). In general, the fraction of ferrite in the microstructures increased as the cooling rate was decreased.

A quantitative evaluation of the ferrite volume fraction results from the different samples is plotted in Fig. 6. When the cooling rate was less than 1 °C/s, the ferrite volume fraction decreased considerably as the cooling rate was increased. When the cooling rate was between 1 and 2 °C/s, the rate of decrease in the ferrite volume fraction slowed and the ferrite volume fraction decreased more slowly after the cooling rate reached 2 °C/s. In the controlled cooling process, different ferrite volume fractions ranging from 6.69 to 40.53% in the notched specimens and from 14.1 to 39.16% in normal tensile specimens were obtained. As shown in Fig. 4(b), there was a small notch of 2 mm at the center of each specimen. During the heating and cooling process, the thermocouple used for temperature control was welded as close as possible to the notch area without contacting it. Thus, the real cooling rate of the notched area with a smaller diameter was likely different from the set-up cooling rate, resulting in the difference of the ferrite volume fractions between the normal and notched samples. Nevertheless, different tensile specimens with different volume fractions of ferrite in their microstructure were achieved as intended.

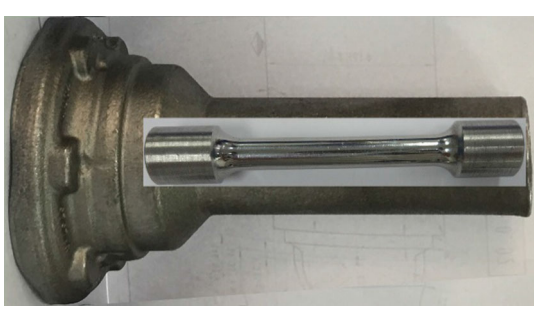

Fig. 12 Location of tensile specimen machined from the hot forging workpiece

3.2 Evaluation of Cold Forgeability

The yield strength and UTS obtained from normal tensile tests are shown in Fig. 7. The data measured at each cooling rate showed good consistency. In general, the downtrend of yield strength resembled that of the UTS as the ferrite volume fraction increased. Ferrite is a typical soft phase with a strength of 280 MPa and a hardness of approximately 80 HB in the microstructure, and its weakening effect on the specimen was clear. When the ferrite volume fraction increased from 14.10 to 39.16%, the yield strength decreased from 459.7 to 344.0 MPa and the UTS decreased from 702.0 to 616.4 MPa. However, the effect on the UTS was relative small, and the UTS value remained stable in the ferrite volume fraction range of 17.2-20.4%.

The results of the elongation rate and percentage reduction in the area from testing of the normal tensile specimens are plotted in Fig. 8. The elongation rate considerably increased with the ferrite volume fraction; the specific value increased from 11.14 to 26.36%. Ferrite with a body-centered cubic form improved the elongation of the whole matrix. The PRA first increased and then decreased as the ferrite volume fraction increased. A peak value of 50.89% was achieved when the ferrite volume fraction was 23.85%. Notably, the relationship between the elongation rate and PRA was different. A possible reason for the different performance of these two plastic indexes is that the tensile specimens with high ferrite volume fraction suffered from a lower cooling rate and a more uniform temperature distribution could be obtained, resulting in a more uniform microstructure over the cross section. This structure promoted elongation deformation of the specimen before necking.

The yield strength is the lowest stress that produces a permanent deformation in a material, which will directly affect the load of cold forging. A large yield strength means a high forging load when the size of the billet and deformation degree in cold forging are the same. Through curve fitting, we identified a power law function, shown in Eq 2, to describe the relationship between the yield strength and ferrite volume fraction. The two independent parameters of the function were determined to be 263.42 and − 0.288 by a fitting process. As shown in Fig. 9, the corresponding R square value was 0.99, which indicates that a close-fitting result was achieved.

$$\sigma_s = 263.42 f_a^{-0.288} \quad \text{(Eq 2)}$$

where σ_s is the yield strength and f_a is the ferrite volume fraction.

As shown in Fig. 10, the fracture strain acts a rough indicator of the formability of a material. The values obtained from the notched tensile specimens increased from 0.256 to 0.388 as the ferrite volume fraction increased from 6.69 to 40.53%. An increase in the ferrite volume fraction of ferritic–pearlitic steel improved its ductility, as expected. Compared

Table 1 Error analysis of modeling predictions and results of tensile tests

	Measured values						
No.	1	2	3	Average	Prediction value	Absolute error	Relative error, %
Yield strength, MPa	410.5	405.7	415.2	410.47	392.14	18.33	4.47
Fracture strain	0.338	0.329	0.352	0.340	0.351	0.011	3.24

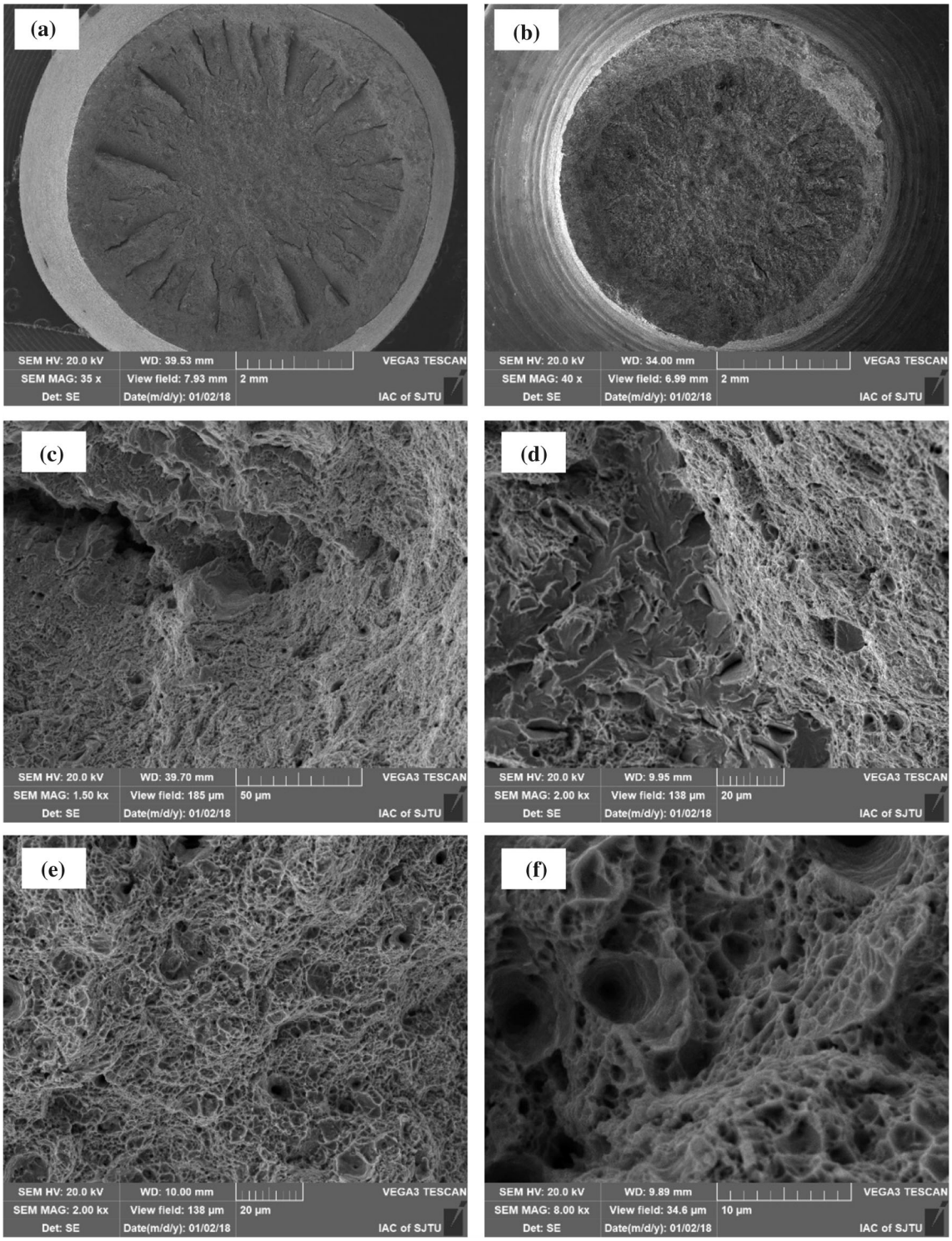

Fig. 13 SEM images of fractured surfaces: (a) normal specimen; (b) notched specimen; (c) edge of normal specimen; (d) edge of notched specimen; (e) center of normal specimen; (f) center of notched specimen

with the PRA measured from the necked specimens, the fracture strain could be determined more precisely because of the homogenous deformation in the local zone.

According to the data distribution, an exponential function, shown by Eq 3, was chosen for the fitting function. As shown in Fig. 11, the three key coefficients were calculated to be − 0.2464, − 4.1894, and 0.4266 by a least-squares method. The linear correlation coefficient R square was larger than 0.98, and there was good agreement between the original data and the fitting function.

$$\varepsilon_f = -0.2464\exp(-4.1894 f_a) + 0.4366 \quad \text{(Eq 3)}$$

Here, ε_f is the fracture strain.

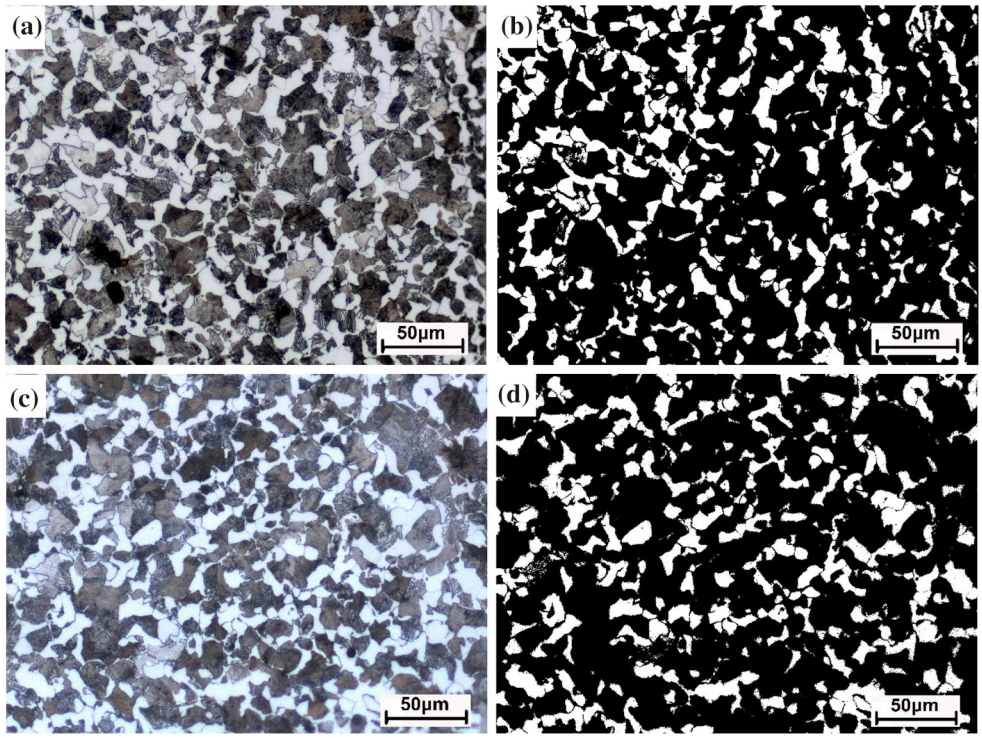

Fig. 14 Metallography of the workpiece: (a) as observed—notched, (b) after binarizing process—notched, (c) as observed—normal, (d) after binarizing process—normal

In this study, the yield strength, indicating deformation resistance, and fracture strain, indicating formability and ductility, were used to evaluate the cold forgeability. As discussed above, the yield strength decreased and the fracture strain increased as the ferrite volume fraction in the dual-phase microstructure increased. Thus, the cold forgeability of the ferrite–pearlite steel was improved as the ferrite volume fraction increased.

3.3 Further Analysis with Real Forged Parts

To evaluate the microstructure generated from the controlled cooling process with residual heat after hot/warm forging and to enable better design of the deformation degree following cold forging, the mathematical relationship between Eq 2 and 3 was used to predict the cold forgeability. To validate the predicting accuracy for the yield strength and fracture strain, three normal and three notched tensile specimens were machined from the rod part of hot forging workpieces. The specimens were then heated up to 1000 °C by induction heating and hot-forged in three stages. After a controlled cooling process in a mesh belt furnace, as shown in Fig. 12, the specimens were tested, and their yield strength and fracture strain were measured. These results are listed in Table 1.

As shown in Fig. 13, the SEM fractography on the tested specimens were conducted and images of fracture surface with different magnification were obtained. From the presented morphologies, the rupture behavior of the specimens shows typical ductile fracture as expected. However, the specific fracture processes of the normal and notched specimens are different. As shown in Fig. 13(a), the macro-morphology of normal specimen presents radial pattern. The secondary cracks start from the position of around 1/2 radius and propagate along the radial direction until the total crack of the specimen. At the outer junction area, there is significantly geometric difference which can be easily observed from the micromorphology illustrated in Fig. 13(c). These secondary cracks are initiated from the micro-voids at the center and speed up the fracture after necking. In general, the rupture is mainly caused by the aggregation of micro-voids, as shown in Fig. 13(e). As for the notched specimen, the radial secondary cracks are hardly initiated because the special geometry of notch, as shown in Fig. 13(b). A typical fracture transition zone is found at the outer junction area and a shear fracture at the outer zone, while a trans-granular shear fracture at the inner zone can be observed from Fig. 13(d). In the center of the notched specimen, the crack is dominated by micro-voids aggregation toughness fracture, as presented in Fig. 13(f).

Metallography samples were cut in the radial direction from broken tensile specimens, and the corresponding microstructures at the center were observed. As shown in Fig. 14(a) and (c), the microstructures presented a typical ferritic–pearlitic dual-phase morphology. The pearlite phase mainly consisted of lamellar pearlite, and its size was similar to that of the ferrite grains. The volume fraction of ferrite was determined to be 25.12% with a standard deviation of 1.20%, based on a previously developed binarization method (Ref 14). Corresponding images of binarizing processed micrographs are shown in Fig. 14(b) and (d).

As shown in Table 1, the average value of the measured yield strength from normal tensile tests was 410.47 MPa and the value of the yield strength, predicted by Eq 2, was 392.14 MPa. The absolute error between the prediction and the measurement was 18.33 MPa, and the relative error was 4.47%. The average fracture strain measured from the notched tensile tests was 0.340, while the predicted value from Eq 3 was 0.351, giving an absolute error of 0.011 and a relative error

of 3.24%. Thus, there is good agreement between the predicted and real tested results.

However, some error existed between the predicted and measured values. As reported in Ref 23, low-yield stress and flow stress increased while the elongation decreased as ferrite grain size decreased within the range of 13.6-0.47 μm. The effect of ferrite grain size on the flow stress was almost independent of the strain rate. The yield strength follows a Hall–Petch-type relationship with respect to the interlamellar spacing, but the UTS and impact toughness did not follow this relationship. The UTS, impact toughness, and ductility remain invariant to the interlamellar spacing below a critical size in nearly fully pearlitic steel (Ref 24). Therefore, the grain size of the ferrite and the interlamellar spacing of pearlite both affect the mechanical properties and the cold forgeability of ferrite–pearlite steel.

Thus, further consideration of the microstructure will improve the prediction accuracy of the mathematical relationship. However, quantitative assessment of the ferrite grain size and interlamellar spacing of pearlite requires detailed analysis, which would be difficult to implement in the process design of combined hot/warm and cold forging. In general, the predicted error of the cold forgeability, based on the ferrite volume fraction of XC45 steel in the dual-phase microstructure, was less than 5%, which is acceptable for industrial forging applications.

As a result, a ferritic–pearlitic microstructure that contained 25.12% ferrite of the hot-forged flange shaft treated by controlled cooling process was obtained. The predicted value of fracture strain was 0.351, with this guide the cold ironing process with a reduction in cross section of 30.5%, where the diameter of the rod was reduced from 42.0 to 35.0 mm, was designed for the part. By the proper design of the combined hot–cold forging with an intermediate controlled cooling process, the automotive flange shaft has been mass produced.

4. Conclusions

We aimed to combine hot/warm and cold forging with an intermediate controlled cooling process to manufacture automobile flange shafts. A medium-carbon steel (XC45) was selected, and the influence of the ferrite–pearlite microstructure on the cold forgeability was investigated. The primary results are as follows:

1. Normal and notched tensile specimens were heated up to 1000 °C and cooled down at seven different cooling rates less than 5 °C/s in a Gleeble 1500 system to simulate real forging conditions. Different ferrite volume fractions ranging from 6.69 to 40.53% in the ferrite–pearlite microstructure were achieved. When the cooling rate was higher than 1.5 °C/s, proeutectoid ferrite appeared as a thin, continuous network at the boundary of former austenite grains. When the cooling rate was lower than 1.5 °C/s, many equiaxed grain geometries, referred to as polygonal ferrite, appeared in the microstructure.
2. The yield strength, UTS, elongation rate, PRA, and fracture strain of the specimens were determined by tensile testing. The yield strength reflects deformation resistance, and the fracture strain reflects formability. These characteristics were selected for evaluation of the cold forgeability. The cold forgeability of the ferritic–pearlitic steel improved as the ferrite volume fraction increased.
3. The yield strength determined from normal tensile testing decreased from 459.7 to 344.0 MPa when the ferrite volume fraction increased from 14.10 to 39.16%. The relationship between the yield strength and the ferrite volume fraction was determined as: $\sigma_s = 263.42 f_a^{-0.288}$. The measured average value of the specimens machined from real hot-forged parts was 410.47 MPa, while the predicted value was 392.14 MPa. The relative error between the prediction and the actual result was 4.47%.
4. The fracture strain from notched tensile testing increased from 0.256 to 0.388 as the ferrite volume fraction increased from 6.69 to 40.53%. The relationship between the fracture strain and ferrite volume fraction was fitted as: $\varepsilon_f = -0.2464 \exp(-4.1894 f_a) + 0.4366$. The average value from real measurements was 0.340 and the predicted value was 0.351, giving an absolute error of 0.011. Thus, there was good agreement between the predicted and real tested results.
5. With an error less than 5%, the mathematical relationship for predicting the cold forgeability is acceptable for industrial applications. With guide of the predicted value, a successful cold ironing process with a deformation degree of 30.5% was designed for the mass production of the automotive flange shaft.

Acknowledgments

This work was supported by the National Natural Science Foundation of China (No. 51475294).

References

1. T.W. Ku, L.H. Kim, and B.S. Kang, Process Simplification of Multistage Forging for the Outer Race of a CV Joint, *Mater. Manuf. Processes*, 2014, **29**(2), p 85–92
2. D.H. Park and H.H. Kwon, Development of Automobile Engine Mounting Parts Using Hot-Cold Complex Forging Technology, *IJPEM Green Technol.*, 2016, **2**(3), p 179–184
3. Y.C. Chang, Z.M. Hu, B.S. Kang, and T.A. Dean, A Study of Cold Ironing as a Post-process for Net-Shape Manufacture, *Int. J. Mach. Tools Manuf.*, 2002, **42**(8), p 945–952
4. Z. Li, B. Wang, W. Ma, and L. Yang, Comparison of Ironing Finishing and Compressing Finishing as Post-forging for Net-Shape Manufacturing, *Int. J. Adv. Manuf. Technol.*, 2016, **9**(86), p 3333–3343
5. M. Umemoto, G.Z. Hai, and I. Tamura, Effect of Cooling Rate on Grain Size of Ferrite in a Carbon Steel, *Materi. Sci. Technol.*, 1987, **3**(4), p 249–255
6. M.C. Zhao, K. Yang, F.R. Xiao, and Y.Y. Shan, Continuous Cooling Transformation of Undeformed and Deformed Low Carbon Pipeline Steels, *Mater. Sci. Eng. A*, 2003, **355**(1), p 126–136
7. L. Ceschini, A. Marconi, C. Martini, A. Morri, and A. Di Schino, Tensile and Impact Behaviour of a Microalloyed Medium Carbon Steel: Effect of the Cooling Condition and Corresponding Microstructure, *Mater. Des.*, 2013, **45**, p 171–178
8. L.I. Gladshtein, N.P. Larionova, and B.F. Belyaev, Effect of Ferrite–Pearlite Microstructure on Structural Steel Properties, *Metallurgist*, 2012, **56**, p 1–12
9. M.R. Akbarpour and A. Ekrami, Effect of Ferrite Volume Fraction on Work Hardening Behavior of High Bainite Dual Phase (DP) Steels, *Mater. Sci. Eng. A*, 2008, **477**(1), p 306–310
10. N. Saeidi and A. Ekrami, Comparison of Mechanical Properties of Martensite/Ferrite and Bainite/Ferrite Dual Phase 4340 steels, *Mater. Sci. Eng. A*, 2009, **523**(1), p 125–129

11. D. Rasouli, S.K. Asl, A. Akbarzadeh, and G.H. Daneshi, Effect of Cooling Rate on the Microstructure and Mechanical Properties of Microalloyed Forging Steel, *J. Mater. Process. Technol.*, 2008, **206**(1), p 92–98
12. A. Babakhani, S.M.R. Ziaei, and A.R. Kiani-Rashid, Investigation on the Effects of Hot Forging Parameters on the Austenite Grain Size of Vanadium Microalloyed Forging Steel (30MSV6), *J. Alloys Compd.*, 2010, **490**(1), p 572–575
13. S. Herbst, M. Schledorn, H. Maier, A. Milenin, and F. Nürnberger, Process Integrated Heat Treatment of a Microalloyed Medium Carbon Steel: Microstructure and Mechanical Properties, *J. Mater. Eng. Perform.*, 2016, **25**(4), p 1453–1462
14. C.L. Hu, Z. Zhao, A.J. Gong, and W.B. Shi, Effect of Warm Deformation Parameters and Cooling Rates on the Recrystallization Transformation Microstructure in 40Cr Steel, *J. Mater. Eng. Perform.*, 2015, **24**(1), p 505–516
15. J. Trzaska, A. Jagiello, and L.A. Dobrzański, The Calculation of CCT Diagrams for Engineering Steels, *Arch. Mater. Sci. Eng.*, 2009, **39**(1), p 13–20
16. R.K. Guduru, K.A. Darling, R. Kishore, R.O. Scattergood, C.C. Koch, and K.L. Murty, Evaluation of Mechanical Properties Using Shear-Punch Testing, *Materi. Sci. Eng. A*, 2005, **395**(1), p 307–314
17. M. Olasolo, P. Uranga, J.M. Rodriguez-Ibabe, and B. López, Effect of Austenite Microstructure and Cooling Rate on Transformation Characteristics in a Low Carbon Nb–V Microalloyed Steel, *Materi. Sci. Eng. A*, 2011, **528**(6), p 2559–2569
18. E. Ulvan and A. Koursaris, Metal Formability in Bulk Deformation Processes, *JOM*, 1983, **35**(12), p 20–26
19. E. Karadeniz, Influence of Different Initial Microstructure on the Process of Spheroidization in Cold Forging, *Mater. Des.*, 2008, **29**(1), p 251–256
20. J.C. Gelin, J. Oudin, and Y. Ravalard, Influence De Quelques Parametres Metallurgiques Sur La Rupture Ductile des Acieres a bas de Moyen carbone, *MES Rev. Metall*, 1984, **4/84**, p 169–179
21. G. Krauss and S.W. Thompson, Ferritic Microstructures in Continuously Cooled Low-and Ultralow-Carbon STEELS, *ISIJ Int.*, 1995, **35**(8), p 937–945
22. B. Eghbali and A. Abdollah-Zadeh, Influence of Deformation Temperature on the Ferrite Grain Refinement in a Low Carbon Nb–Ti Microalloyed Steel, *J. Mater. Process. Technol.*, 2006, **180**(1), p 44–48
23. N. Tsuchida, H. Masuda, Y. Harada, K. Fukaura, Y. Tomota, and K. Nagai, Effect of Ferrite Grain Size on Tensile Deformation Behavior of a Ferrite–Cementite Low Carbon Steel, *Mater. Sci. Eng. A*, 2008, **488**(1), p 446–452
24. O.P. Modi, N. Deshmukh, D.P. Mondal, A.K. Jha, A.H. Yegneswaran, and H.K. Khaira, Effect of Interlamellar Spacing on the Mechanical Properties of 0.65% C Steel, *Mater. Charact.*, 2001, **46**(5), p 347–352